Electronic Supplementary Information (ESI)

Balancing protection and charge transport of aggregation-induced delayed fluorescence luminogen for optimizing aqueous electrochemiluminescence

Yongjing Chen, [a] Junting Hong, [c] Xianxi Liang, [a] Shulin Li, [a] Yuwei Zhang, [c] Xingzi Zou, [a] Yu Bao, [a] Zujin Zhao, *[d] Li Niu, [a,e] and Baohua Zhang *[a,b]

[a] Center for Advanced Analytical Science, Guangzhou Key Laboratory of Sensing Materials and Devices, Guangdong Engineering Technology Research Center for Photoelectric Sensing Materials and Devices, c/o School of Chemistry and Chemical Engineering, Guangzhou University, Guangzhou 510006, China. E-mail: ccbhzhang@gzhu.edu.cn

[b] State Key Laboratory of Organic Electronics and Information Displays & Institute of Advanced Materials (IAM), Nanjing University of Posts & Telecommunications, Nanjing 210023, China.

[c] GDMPA Key Laboratory for Process Control and Quality Evaluation of Chiral Pharmaceuticals, and Guangzhou Key Laboratory of Analytical Chemistry for Biomedicine, School of Chemistry, South China Normal University, Guangzhou 510006, China.

[d] State Key Laboratory of Luminescent Materials and Devices, Guangdong Provincial Key Laboratory of Luminescence from Molecular Aggregates, South China University of Technology, Guangzhou 510640, China. E-mail: mszjzhao@scut.edu.cn

[e] School of Chemical Engineering and Technology, Sun Yat-sen University, Zhuhai, 519082, China

1. Materials

Poly(styrene-co-maleic anhydride) (PSMA) (average Mn: 1900) and tetrahydrofuran (THF, ≥ 99.9%) were purchased from Sigma-Aldrich Co. Ltd. Triethanolamine (TEOA, ≥ 98%) and tetra-n-butylammonium hexafluorophosphate (TBAPF6, 98%) were obtained from Alfa Co. Ltd. Phosphate-buffered saline (PBS, pH 7.42) was prepared by mixing 0.1 M KNO_3 with 0.1 M K_2HPO4 and 0.1 M KH_2PO4, while the filter membrane was sourced from local reagent suppliers. All other reagents used were of analytical grade, and ultrapure water was employed throughout the study.

2. Synthesis and characterization

The compound BCP-BP-DMAC was synthesized by Zhao's group using a method analogous to the synthesis route previously reported for CDBP-BP-DMAC [1], with the modification that the 9,9′-(2,2′-dimethyl-[1,1′-biphenyl]-4,4′-diyl)bis(9H-carbazole) (CDBP) molecule was replaced by 9,9′-diphenyl-9H,9′H-3,3′-bicarbazole (BCP) in the initial step of the synthesis.

BCP-BP-DMAC:

^{1}H NMR (600 MHz, Chloroform-*d*) δ 8.90 (d, *J* = 1.6 Hz, 1H), 8.57 (d, *J* = 1.7 Hz, 1H), 8.50 (d, *J* = 1.8 Hz, 1H), 8.27 (d, *J* = 7.6 Hz, 1H), 8.21 – 8.15 (m, 2H), 8.09 (dd, *J* = 8.7, 1.7 Hz, 1H), 7.88 (dd, *J* = 8.5, 1.8 Hz, 1H), 7.81 (dd, *J* = 8.4, 1.9 Hz, 1H), 7.73 – 7.64 (m, 9H), 7.61 – 7.46 (m, 12H), 7.06 (ddd, *J* = 8.4, 7.2, 1.6 Hz, 2H), 6.99 (td, *J* = 7.5, 1.3 Hz, 2H), 6.43 (dd, *J* = 8.2, 1.2 Hz, 2H), 1.74 (s, 6H).

^{13}C NMR (151 MHz, Chloroform-*d*) δ 195.71, 144.75, 144.02, 141.40, 141.28, 140.92, 140.60, 140.20, 138.45, 137.73, 137.00, 135.53, 133.80, 132.75, 132.62, 131.21, 131.05, 130.49, 130.19, 129.96, 129.33, 128.90, 128.24, 127.53, 127.12, 127.10, 126.73, 126.47, 126.41, 126.16, 125.78, 125.33, 124.05, 123.93, 123.84, 123.52, 123.42, 121.47, 121.01, 120.48, 120.29, 120.09, 119.27, 118.95, 114.33, 110.63, 110.16, 109.95, 109.69, 36.08, 31.14.

HRMS calculated for $C_{58}H_{41}N_3O$ $[M+Na]^+$ 818.3098, found 818.3140. Elemental Analysis for $C_{58}H_{41}N_3O$: C, 87.52; H, 5.19; N, 5.28; O, 2.01.

3. Preparation of BCP-BP-DMAC NPs

Aqueous solutions of BCP-BP-DMAC-based nanoparticles (NPs) with varying specific weight ratios were prepared via the nanoprecipitation method [2-4], where the luminescent AIDF material BCP-BP-DMAC luminogen served as the core and insulating PSMA as

the capping agent. The procedure involved initially dissolving 4 mg of BCP-BP-DMAC and 4 mg of PSMA independently in 2 mL of THF to obtain 2 mg/mL mother solutions, which were thoroughly stirred to ensure complete dissolution. Subsequently, the concentration of BCP-BP-DMAC was fixed at 100 μg/mL while PSMA was adjusted to prepare 2 mL of precursor solutions with specific BCP-BP-DMAC:PSMA weight ratios (ωt %:ωt %) of 1:0 (bare NPs), 2:1, 1:3, and 1:5, respectively. The resulting dispersion underwent standard rotary evaporation at 60 °C to remove THF, yielding a concentrated NPs aqueous solution, which was then filtered through a 0.34 μm membrane to remove larger NPs and subsequently diluted to obtain the final AIDF NPs.

4. Theoretical calculation

All calculations were performed using the Gaussian 16 software package, where the ground-state and excited-state geometries were obtained through Density Functional Theory (DFT) and Time-Dependent DFT (TD-DFT) calculations, respectively, employing the B3LYP functional and 6-31G(d,p) basis set under gas-phase conditions. Subsequently, Multiwfn (version 3.8(dev)[5]) and VMD (version 1.9.3) software packages were utilized for wavefunction analysis, followed by visualization of the frontier molecular orbitals and Natural Transition Orbital (NTO) analysis.

5. Device preparation and characterization

To initiate the process, single-component solutions of BCP-BP-DMAC or (3,5-di(9H-carbazol-9-yl)phenyl)diphenylsilane (SimCP2) (10 mg/mL in chlorobenzene) were prepared in an N_2-filled glovebox and thoroughly dissolved via successive heating and stirring at 50°C for 2 hours. Subsequently, blended solutions at varying SimCP2 ratios (100-x:x, x = 10–100 wt.%) were prepared by combining these solutions as required. For device fabrication, ITO-coated glass substrates (ITO thickness = 110 nm, sheet resistance = 15 Ω/sq) were cleaned and dried using routine methods, followed by UV-ozone treatment in air for 25 minutes. A water dispersion of poly(3,4-ethylenedioxythiophene):poly(styrene sulfonate) (PEDOT:PSS) (Clevios PVP AI4083, Heraeus) was then spin-coated onto the ITO substrate and dried in an air oven at 120°C for 30 minutes, resulting in a PEDOT:PSS layer with a thickness of approximately 50 nm. The device samples were subsequently transferred into an N_2-filled glovebox. The SimCP2:BCP-BP-DMAC blended solutions were spin-coated onto the ITO/PEDOT:PSS surface at 1500 rpm for 1 minute, followed by thermal annealing at

100°C for 30 minutes to obtain an emissive layer with a thickness of ~40 nm. Finally, the samples were loaded into a thermal evaporation chamber (Angstrom Engineering Corp., Canada, EVOVAC) for sequential deposition of bis(2-(diphenylphosphino)phenyl) ether oxide (DPEPO) (10 nm), 1,3,5-tri(m-pyrid-3-yl-phenyl)benzene (TmPyPB) (50 nm), LiF (1 nm), and Al (100 nm). The base pressure during thermal evaporation was maintained below 5×10^{-6} mbar, with a deposition rate of 0.1 nm/s. The emissive area of each device (3.5×4 mm^2) was defined by the overlap between the Al top electrode and the ITO bottom electrode. All preparation steps, except for the ITO and PEDOT:PSS layers, were performed under N_2 protection in a glovebox (mBraun UNIlab, Shanghai; [O_2] < 0.1 ppm, [H_2O] < 0.1 ppm).

The as-fabricated OLEDs were characterized using commercial OLED testing equipment (FS-2000TR, Fstar, Soochow, China), where a Keithley 2400 current-voltage source and a high-resolution spectroradiometer (CS2000A) were integrated and controlled by custom software. Luminance and electroluminescence (EL) spectra were directly acquired using the CS2000A during measurement. The OLEDs were tested unencapsulated in ambient air conditions, and their external quantum efficiency (EQE) performance parameters were calculated under the standard assumption of Lambertian emission characteristics.

6. Instrumental analysis

^{1}H and ^{13}C NMR spectra were recorded on Bruker AVANCE NEO 600MHz spectrometer. High resolution mass spectra (HRMS) were recorded on a GCT premier CAB048 mass spectrometer operating in MALDI-TOF mode. TEM experiments on NPs were performed using a Talos F200S G2 transmission electron microscope (Thermo Fisher Scientific) with an accelerating voltage of 200 kV. UV-Vis absorption measurements were performed using a UV-1780 UV-VIS spectrophotometer (Shimadzu Co.). Photoluminescence (PL) studies were carried out using an Edinburgh Fluorescence Spectrometer (FLS1000) with a light source consisting of a Xe2 xenon lamp and picosecond pulsed LEDs (EPLED-365) for steady state PL and transient PL measurements, respectively. The absolute PL quantum efficiency (Φ_{PL}) of the samples of interest was achieved by using an integrating sphere attachment coupled to the FLS1000 system and controlled by the same commercial software.

All electrochemical tests were conducted using a classic three-electrode system., in which the glassy carbon electrode (GCE, diameter = 4 mm) was sequentially polished with 0.3 μm and 0.05 μm alumina powder, followed by repeated ultrasonic cleaning with ultrapure water and ethanol. The electrode surface was then dried under a nitrogen stream before use. For ECL test, the AIDF-NPs modified GCE served as the working electrode, a Pt wire as the counter electrode, and either a silver wire or an Ag/AgCl electrode (saturated with KCl) as the reference electrode. The CV tests of BCP-BP-DMAC were conducted using 0.1 M $TBAPF_6$ as the supporting electrolyte and ultra-dry dichloromethane as the solvent, with a BCP-BP-DMAC concentration of 1 mM and a scan rate of 100 mV/s. The CV measurements were performed in a glovebox under a nitrogen atmosphere.

To evaluate the double-layer capacitances (Cdl) [6, 7] of these AIDF-NPs modified GCE, CV scanning under different scan rates (from 25 to 150 mV s^{-1}) in the potential region of -0.1 ~ -0.3 V (vs. Ag/AgCl) was performed, in which the test environment is the same as those for the aqueous ECL.

The EIS measurements were conducted as follows: 40 μL of a 0.2 mg/mL AIDF-NPs dispersion was carefully dispensed onto the surface of a pretreated glassy carbon electrode (GCE) using a micropipette. The deposited solution was then dried under an infrared lamp to form a uniform film, resulting in an AIDF NPs-modified GCE. The EIS measurements were performed in a PBS solution containing 10 mM $[Fe(CN)_6]^{3-/4-}$ as the redox probe.

The ECL tests were performed on an MPI-EII multifunctional electrochemiluminescence analysis system (Xi′an Remax, China). The photomultiplier tube (PMT) high voltage was set to 800 V, and the sweep rate was 200 Mv/s. A 40 μL aliquot of AIDF NPs-modified dried GCE served as the working electrode, while a Pt wire electrode and an Ag/AgCl electrode (saturated with KCl) were used as the auxiliary counter electrode and reference electrode, respectively. The three-electrode system was immersed in a PBS solution containing 50 mM co-reactant TEOA, and the ECL tests of a series of AIDF-NPs were conducted with the potential window set at 0 to +1.6 V. All tests were performed at room temperature under anodic ECL conditions. Using the same three-electrode system, ECL spectra were acquired using an FLS1000 spectrometer with the constant potential set at +1.6 V (vs. Ag/AgCl). The ECL efficiency (Φ_{ECL}) of the AIDF-NPs was calculated as follows:

$$\Phi_{ECL} = \Phi_{ECL}^{o} \times \left[\left(\frac{\int_0^t I dt}{\int_0^t i dt} \right) \Big/ \left(\frac{\int_0^t I^o dt}{\int_0^t i^o dt} \right) \right]$$

where Φ_{ECL} and Φ_{ECL}^{o} are the ECL efficiencies of the target and reference samples, respectively; $\int_0^t I dt$ and $\int_0^t I^o dt$ represent the integrated ECL intensity (number of photons) for the target and reference samples; $\int_0^t i dt$ and $\int_0^t i^o dt$ represent the integrated current (number of electrons) for the target and reference samples. In this work, the Φ_{ECL} of bare NPs under scanning (0 to +1.6 V) in PBS buffer (pH 7.42) with 50 mM TEOA was used as the reference value (Φ_{ECL}^{o}), and it was defined as 1.00.

Supplementary Notes

Note 1:

Compared to CDBP, the 3,3'-directly bonded structure of BCP can enhance molecular rigidity and π-conjugation continuity, leading to more extensive frontier orbital delocalization. It is excepted such novel donor-acceptor-donor′ (D-A-D′) molecule design can achieve efficient AIDF property with suppressed non-radiative vibration decay.

Note 2:

In view of an excellent EQE performance achieved for BCP-BP-DMAC, it verified that under electroluminescence (EL) driving conditions, [8] efficient triplet exciton harvesting is realized for this AIDF luminogen while the closely packed situation is constructed at an optimal doping concentration. Achieving a qualified AIDF OLED indicates it is feasible to use BCP-BP-DMAC to construct an efficient AIDF-ECL if its redox and triplet-harvesting capability are also satisfied in aqueous electrolyte media.[9] It thus inspires us to further evaluate its electrochemical and AIDF photophysical properties in aqueous ECL media as follows.

Note 3:

Importantly, a sufficient encapsulation of PSMA renders the resultant AIDF-NP air-stable. For instance, the comparisons of PL transient curves of 1:3 AIDF-NP confirmed that oxygen or air environments has a bare influence on its AIDF emission property (Fig. S14, ESI).

Note 4:

As for these 2:1, 1:3 and 1:5 AIDF-NPs with comparable particle sizes, the double-

layer capacitance (Cdl) of these samples was further measured (Fig. S15, ESI), which shown that they were sequentially increased from 74.5 to 165.1 μF cm^{-2}, indicating the gradual enhancement of electrochemical active area. [6, 7] It confirmed that the increased hydrophilicity is beneficial for charge transportation.

Supplementary Schemes, Figures and Tables

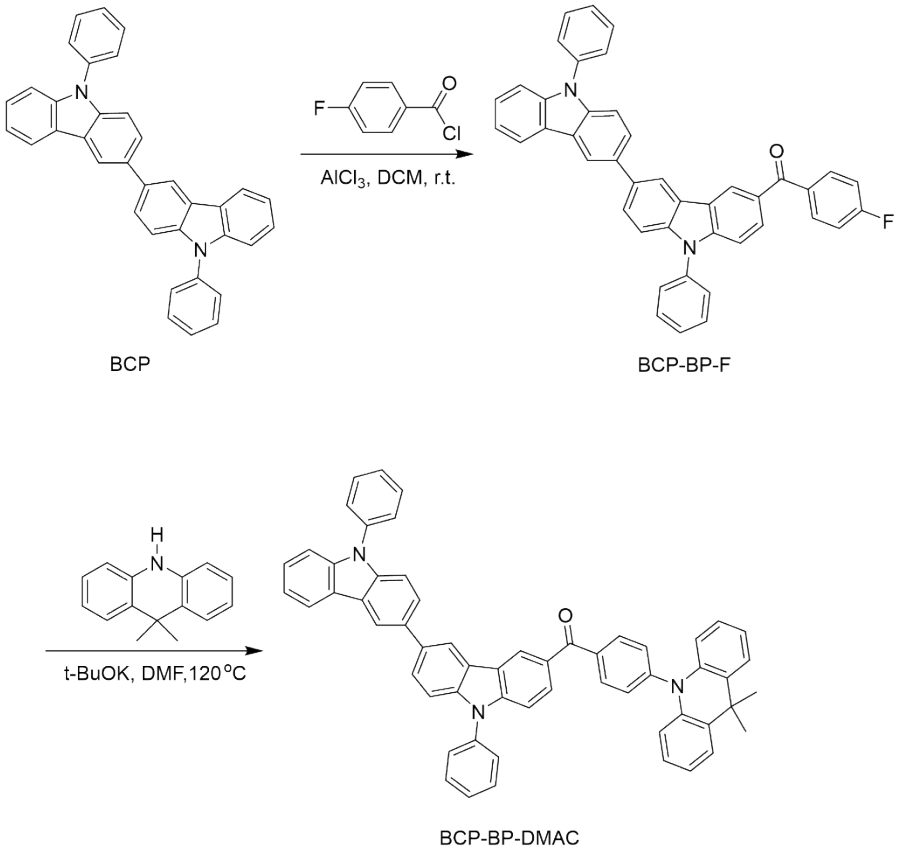

Scheme S1 Schematic synthetic route of BCP-BP-DMAC compound.

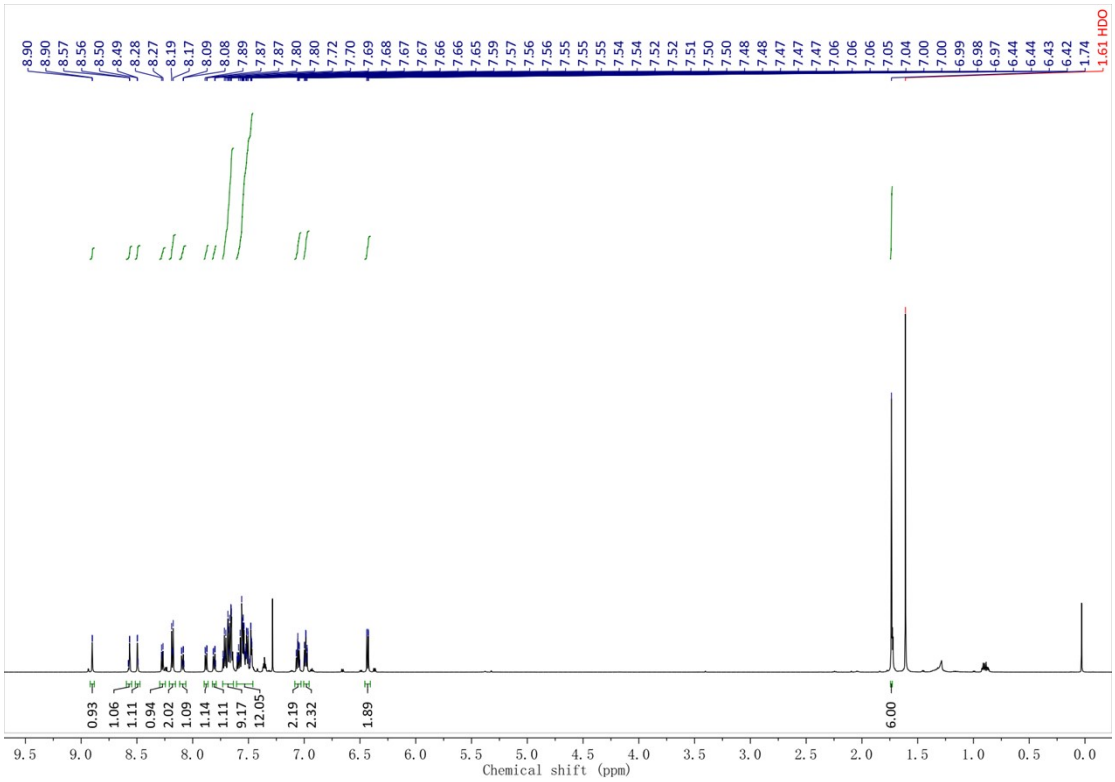

Figure S1 ^{1}H NMR spectrum of the as-synthesized compound.

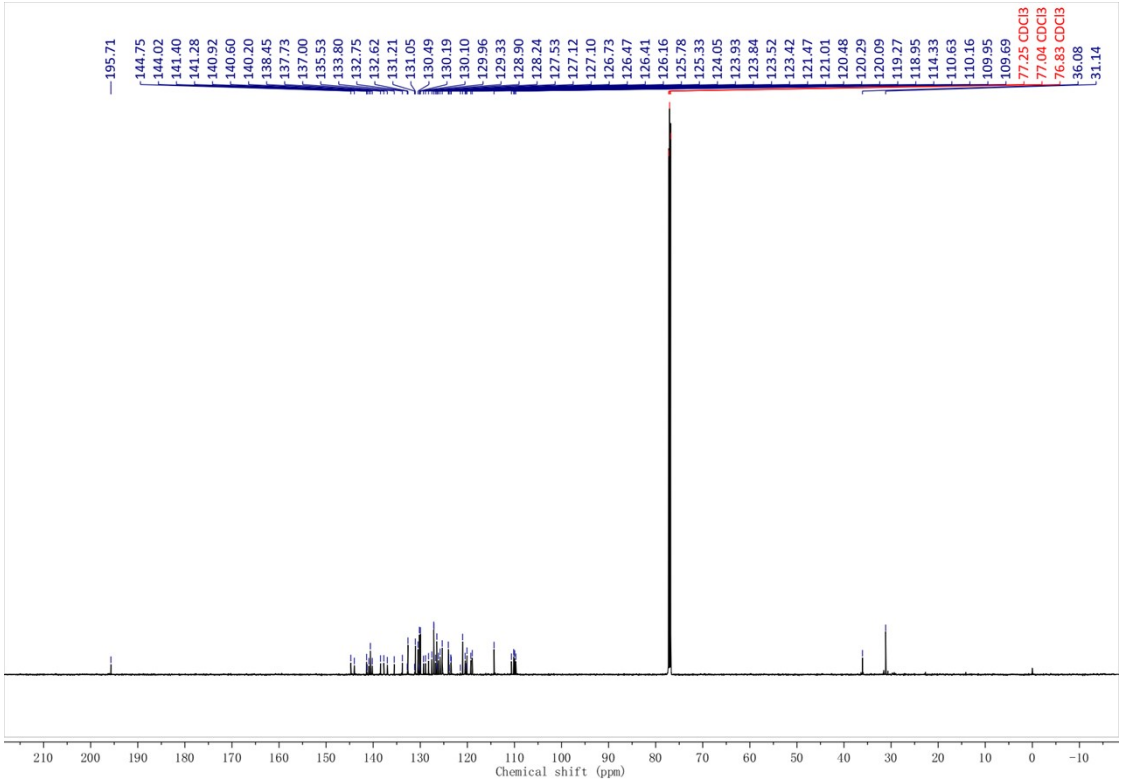

Figure S2 ^{13}C NMR spectrum of the as-synthesized compound.

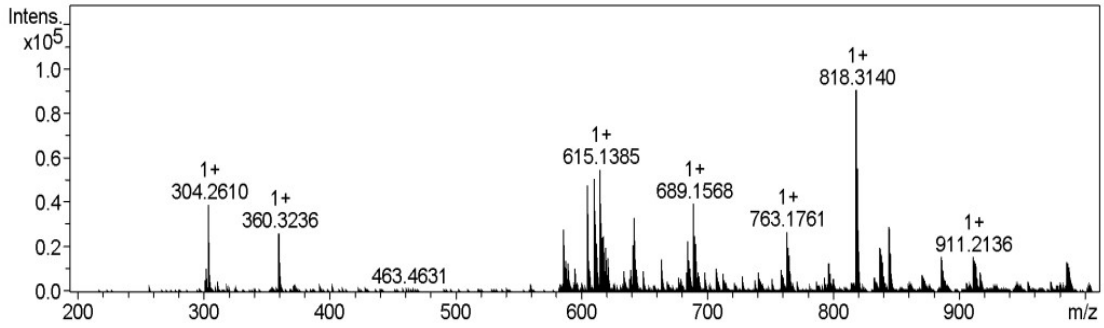

Figure S3 HRMS spectrum of the as-synthesized compound.

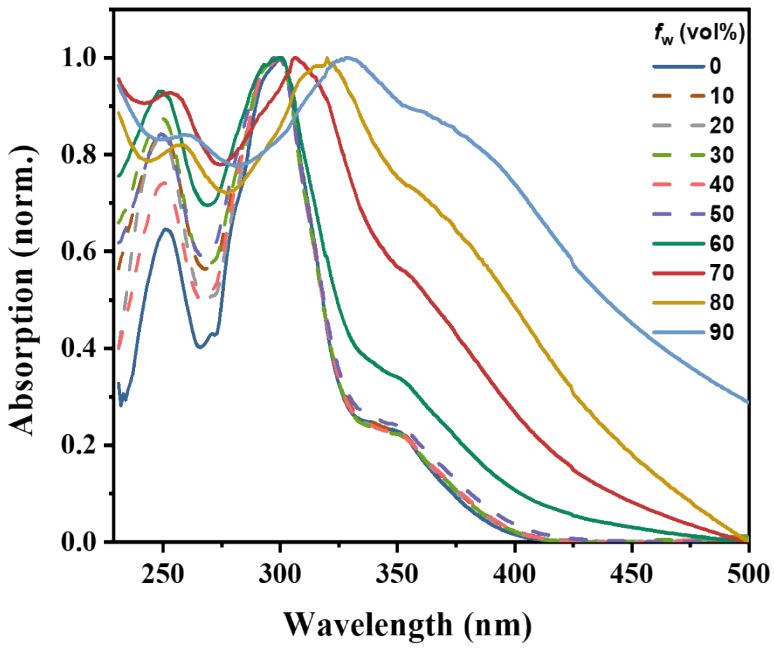

Figure S4 Absorption spectra of BCP-BP-DMAC dissolved in H_2O/THF blended solvent with different water content (excited at 365 nm).

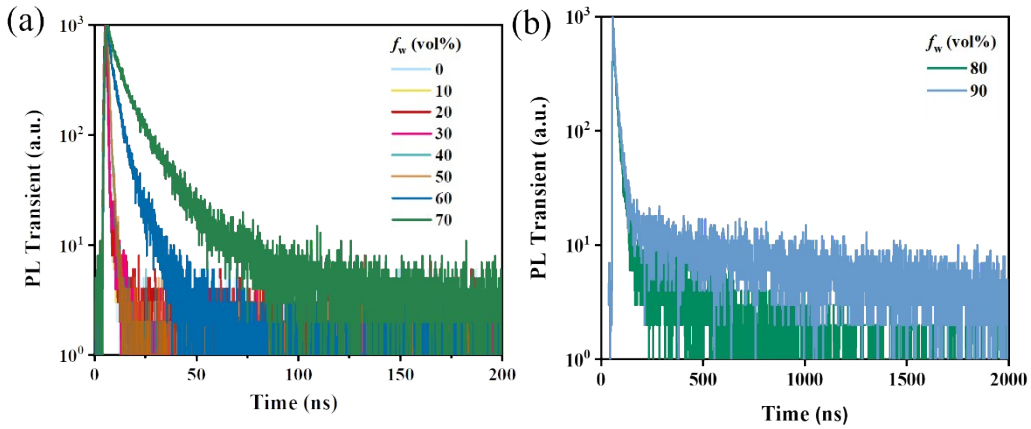

Figure S5 PL transient of BCP-BP-DMAC dissolved in H_2O/THF blended solvent with different water content (excited at 365 nm).

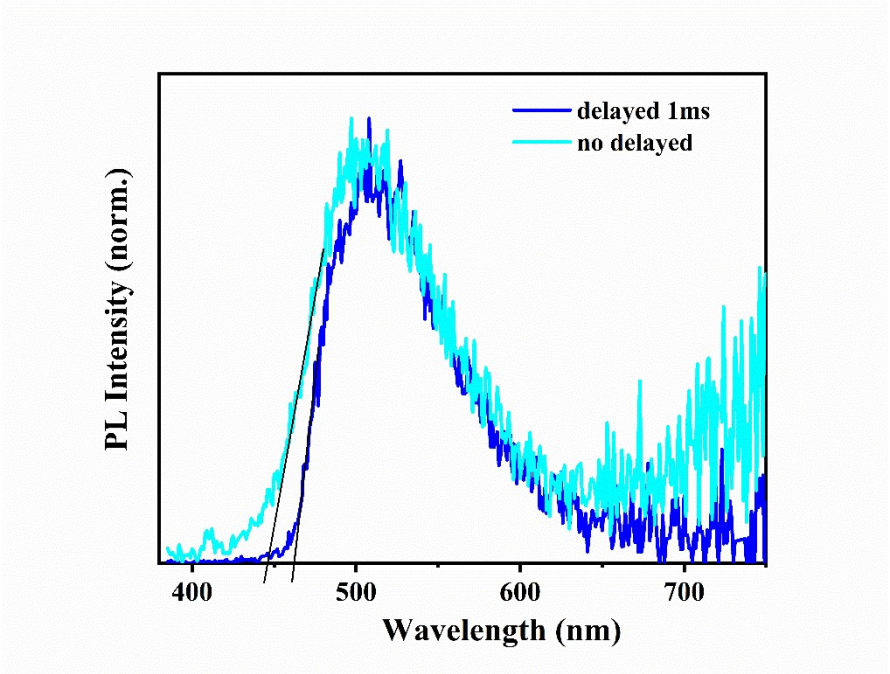

Figure S6 Fluorescent and phosphorescent spectra of BCP-BP-DMAC in H_2O:THF solution (water content: 90%) measured in 77K.

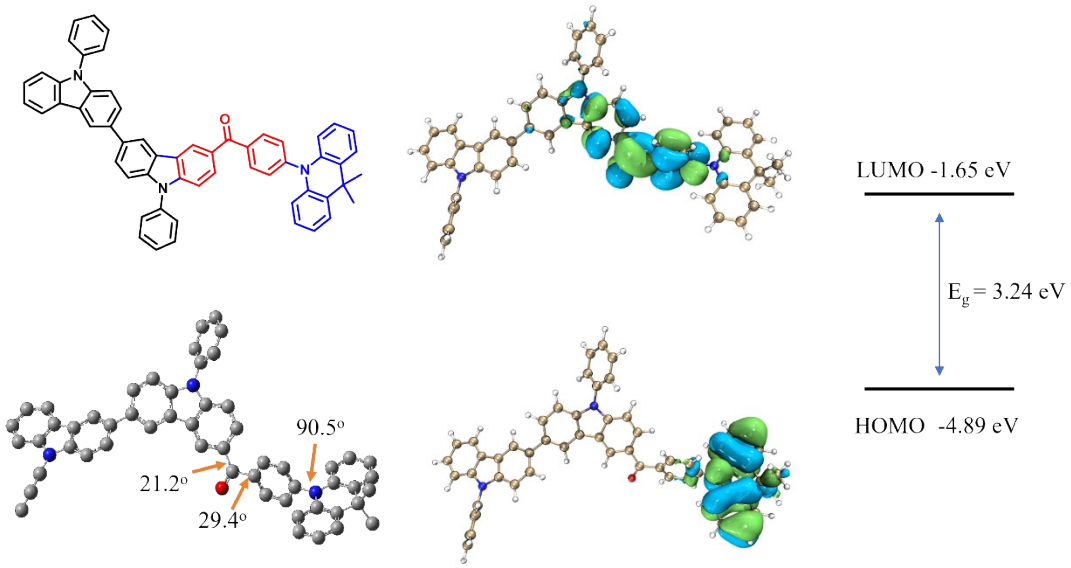

Figure S7 (a) Molecular and ground-state geometry of BCP-BP-DMAC. (b) Frontier orbital plots and their energy gaps calculated by DFT/TD-DFT methods.

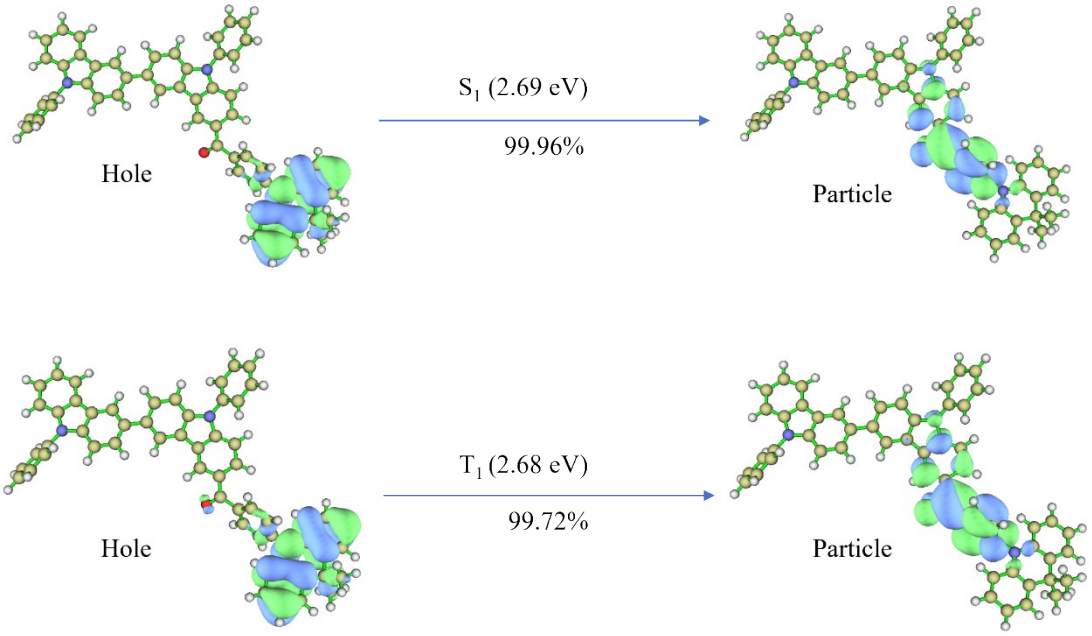

Figure S8 NTO of S_1 and T_1 excited states for BCP-BP-DMAC.

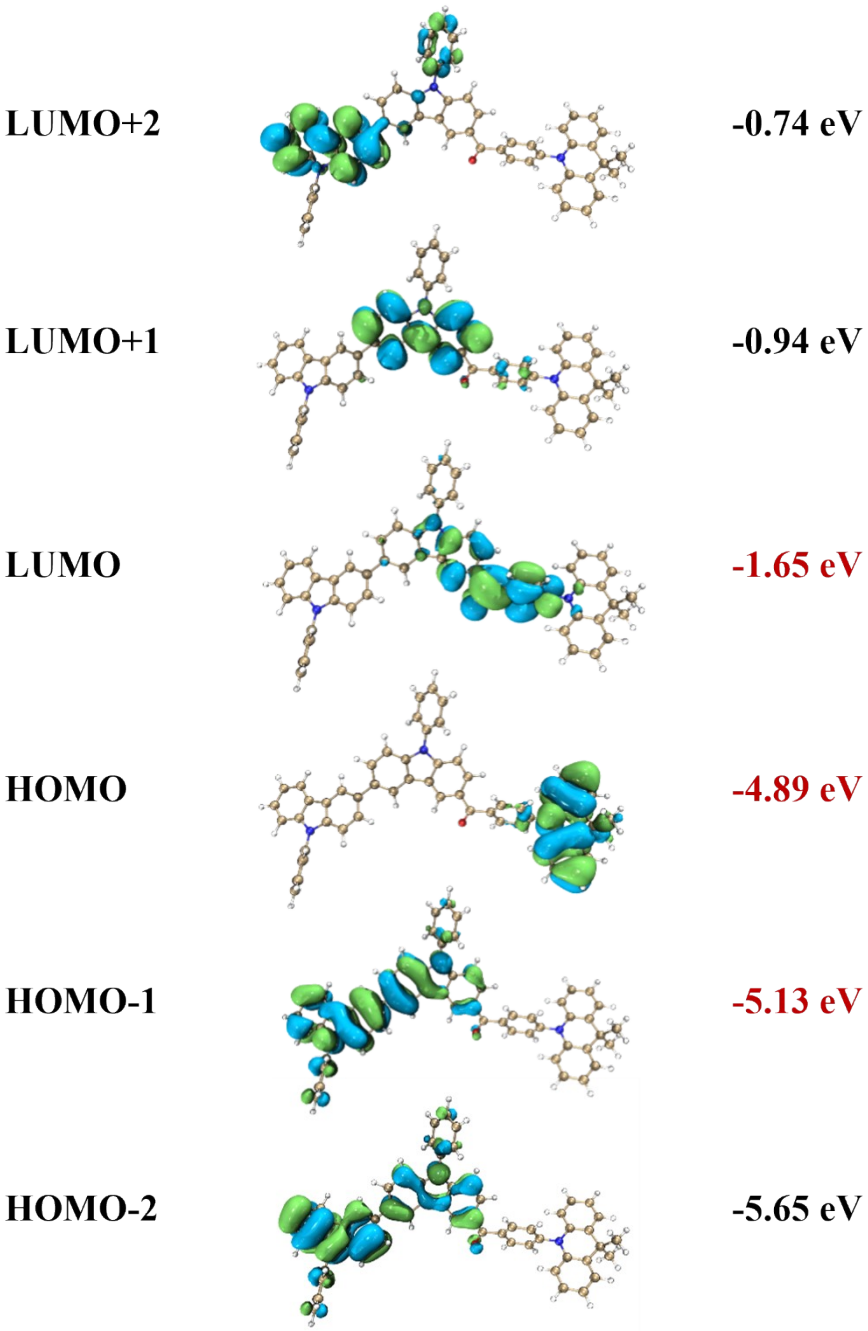

Figure S9 A series of frontiers molecular orbitals of BCP-BP-DMAC.

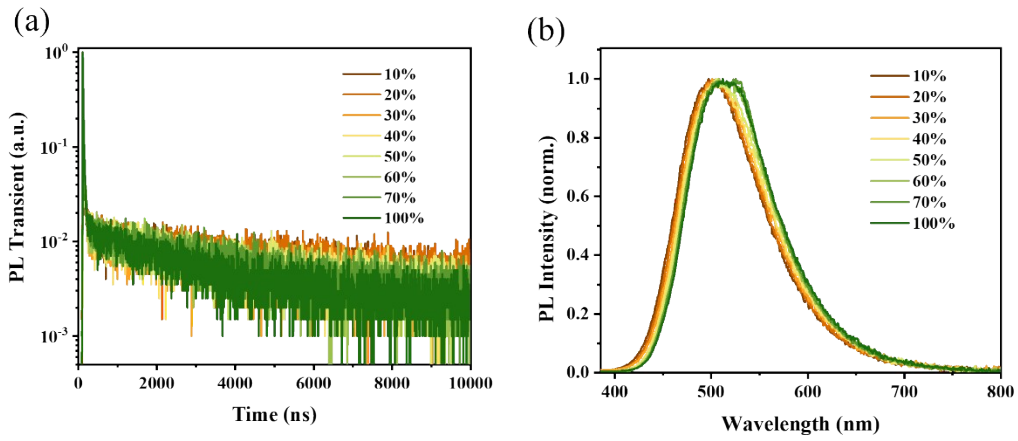

Figure S10 (a) Transient PL and (b) steady-state PL spectra of SimCP2:BCP-BP-DMAC doped films (excited at 365 nm).

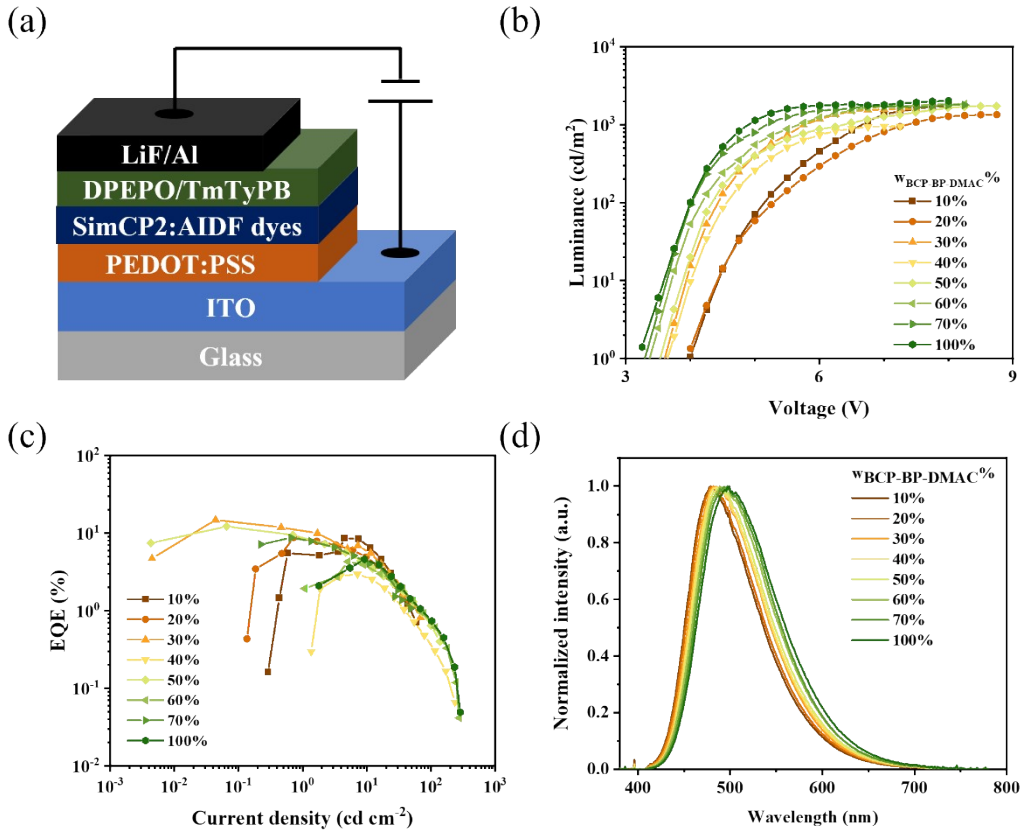

Figure S11 (a) Device structure, (b) luminance-voltage curves, (c) external quantum efficiency (EQE)-current density (J) curves and (d) electroluminescence (EL) spectra of those s-OLEDs using SimCP2:BCP-BP-DMAC doped films (x=10~100 wt.%).

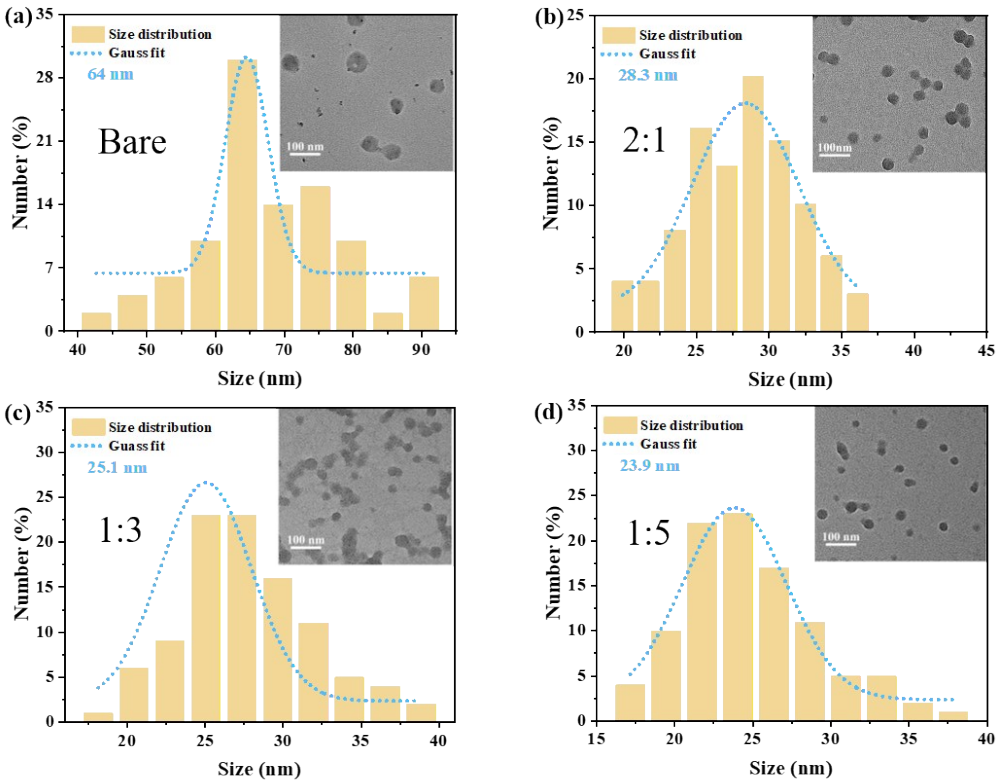

Figure S12 Size distribution and Representative TEM image of BCP-BP-DMAC NPs showing spherical particles of (a) bare (b)2:1 (c)1:3 (d)1:5.

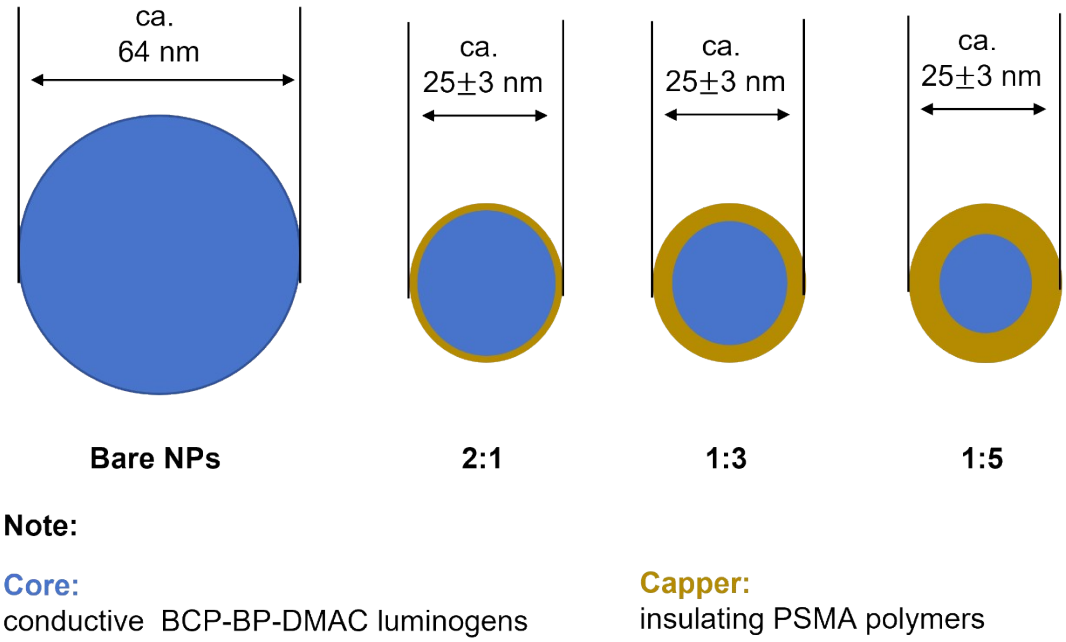

Figure S13 Schematic structure of these NPs concerned, i.e., bare, 2:1, 1:3, 1:5, respectively.

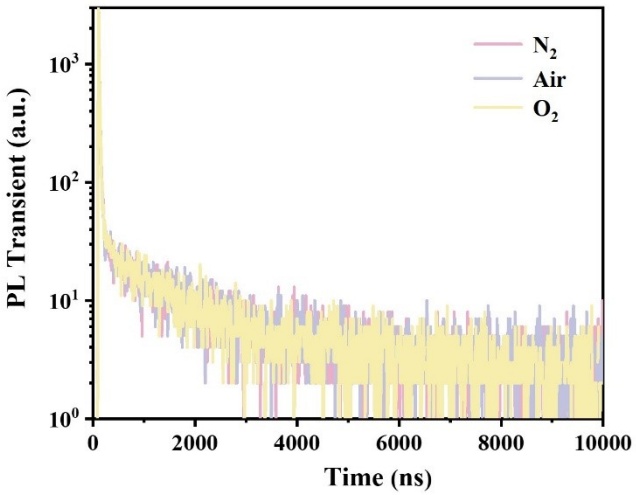

Figure S14 PL transient decay curves of the optimized 1:3 NPs under different atmospheres (excited at 365 nm).

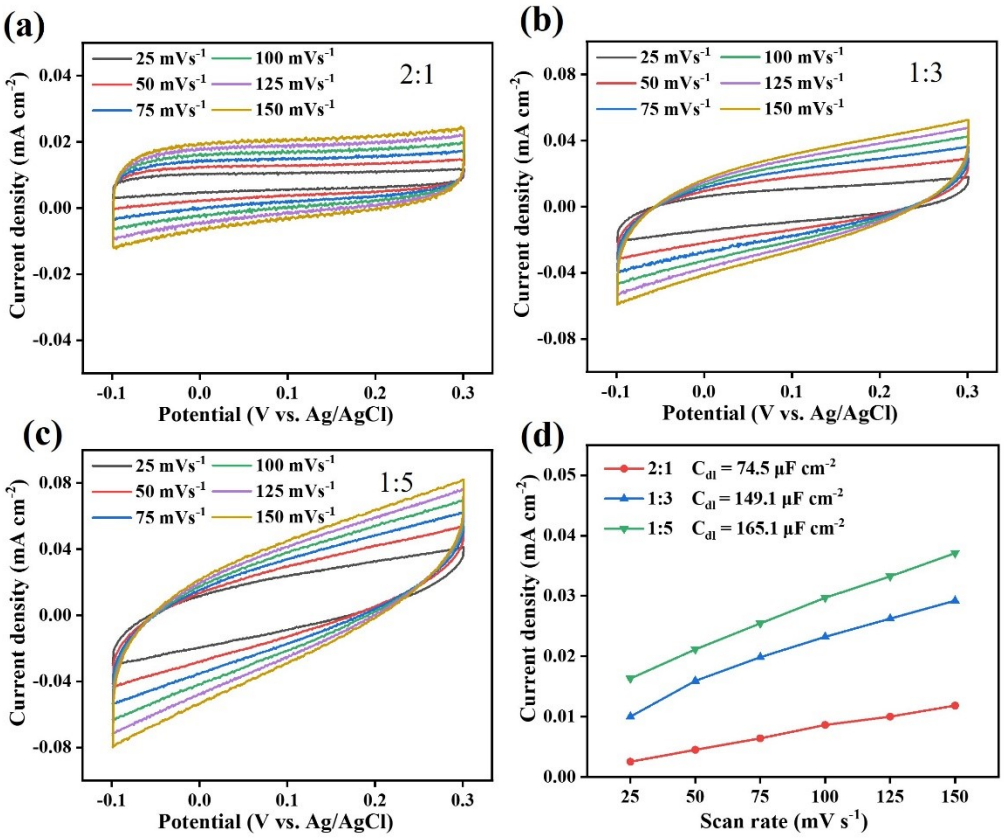

Figure S15 (a) Cyclic voltammetry curves in a non-Faradaic region (different scan rate of 25, 50, 75, 100, 125 and 150 mV s^{-1}) for 2:1 AIDF-NPs (a), 1:3 AIDF-NPs(b) and 1:5 AIDF-NPs (c). (d) Plots of current density (measured at 0.1 V vs Ag/AgCl) of AIDF-NPs modified electrode as a function of scan rate. The average of the absolute value of the slope is taken as the Cdl of these samples.

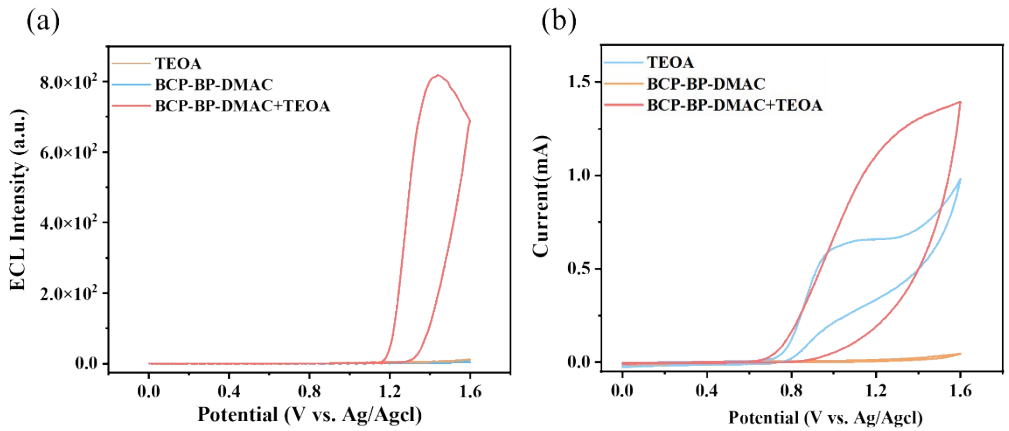

Figure S16 (a) Oxidative-reduction type ECL curves and (b) CVs of 50mM TEOA (orange line), AIDF NPs (black line), AIDF NPs (1:3) and 50mM TEOA (red line) all in PBS (pH=7.42) (scan rage: 0~1.6V, scan rate: 0.5V/s, PMT voltage:800V).

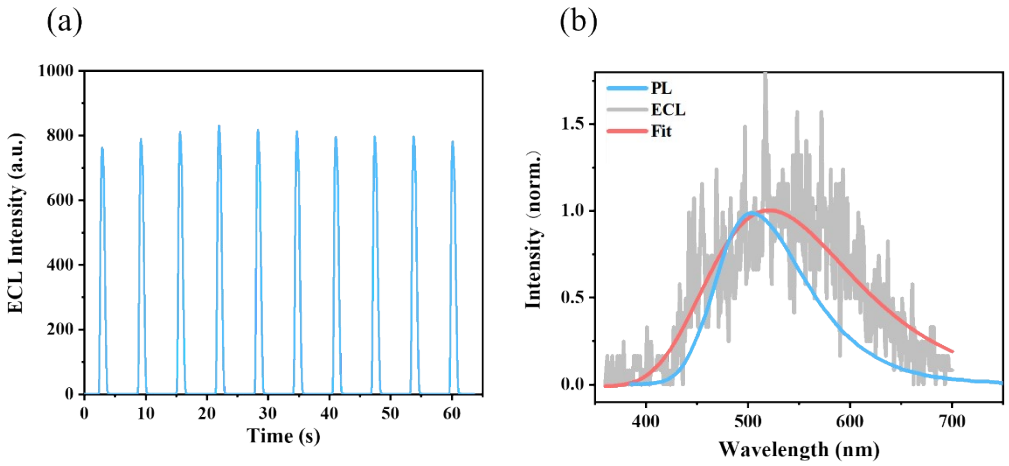

Figure S17 (a) Oxidative-reduction type ECL intensity after continuing 10-times scans. (b) PL Spectra (blue line) and ECL spectrum (red line) of AIDF NPs/TEOA couple (driving potential @ +1.6V vs Ag/AgCl).

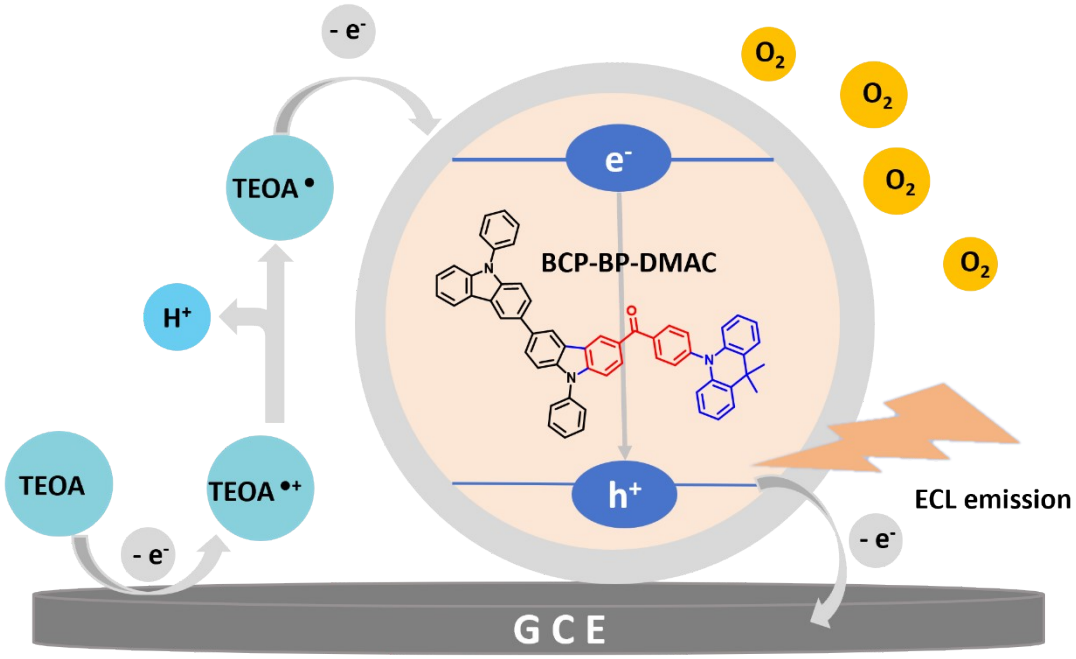

Figure S18 The anodic ECL mechanism of BCP-BP-DMAC NPs in water.

BCP-BP-DMAC NPs − e⁻ →BCP-BP-DMAC NPs•+

TEOA − e⁻ → TEOAH•+

TEOAH•+ → TEOA• + H+

BCP-BP-DMAC NPs•+ + TEOA• → ^{1}BCP-BP-DMAC NPs*(25 %) + ^{3}BCP-BP-DMAC NPs*(75 %) + $TEOA_{ox}$

^{1}BCP-BP-DMAC NPs*(25 %) → BCP-BP-DMAC NPs + *hν*

^{3}BCP-BP-DMAC NPs* (75 %) + Δ → ^{1}BCP-BP-DMAC NPs*(75 %)

^{1}BCP-BP-DMAC NPs* (75 %) → BCP-BP-DMAC NPs + hν

Scheme 2 The schematic mechanisms of ECL.

Table S1 The summarized PL emission and Φ_{PL} parameters of BCP-BP-DMAC dissolved in H_2O/THF blended solvent with different water content (measured in air).

Water content (%)	BCP-BP-DMAC	
	λ_{em}(nm)	Φ_{PL}(%)
0	535	7.19
10	409,597	0.19
20	409,569	0.43
30	409,586	0.13
40	408,432	0.06
50	408,432	0.05
60	409,436,550	2.06
70	533	6.97
80	527	15.12
90	517	31.84

Table S2 Summary of photophysical parameters of SimCP2:BCP-BP-DMAC doped films.

$w_{BCP-BP-DMAC}$%	365nm		295nm		$\tau_{PF}(r_p)$ [ns(%)]	$\tau_{DF}(r_d)$ [ns(%)]
	λ_{PL} [nm]	FWHM [nm]	λ_{PL} [nm]	FWHM [nm]		
10%	501	103	501	103	12.5(19.23)	4578(80.77)
20%	503	103	502	102	12.3(29.81)	3417(70.19)
30%	505	105	504	103	14.6(28.43)	2824(71.57)
40%	506	102	505	104	16.4(27.48)	3120(72.52)
50%	510	105	510	104	16.3(24.14)	3642(75.86)
60%	513	104	514	105	17.8(27.32)	3016(72.68)
70%	514	104	516	103	17.2(28.11)	2909(71.89)
100%	515	106	516	106	17.6(33.54)	2191(66.46)

Table S3 Summary of device performance parameters of s-OLEDs using SimCP2:BCP-BP-DMAC doped emissive layers.

$w_{BCP-BP-DMAC}$%	V_{on} [V]	L [c]	λ_{em}[a] [nm]	FWHM[a] [nm]	EQE_{max} [%]	CE_{max} [cd/A]	PE_{max} [lm/W]	CIE(x,y)[a]
10%	4.0	1715	479	86	8.6	18.8	9.1	(0.19,0.33)
20%	4.0	1342	480	87	8.8	19.7	11.2	(0.19,0.34)
30%	3.6	1591	484	90	14.9	35.1	27.5	(0.20,0.37)
50%	3.5	1730	489	90	12.2	31.9	26.7	(0.22,0.40)
70%	3.3	1836	495	96	8.7	24.8	18.4	(0.23,0.43)
100%	3.2	2017	499	97	4.6	13.8	9.1	(0.24,0.44)

[a] the value at a luminance of 1000 cd/m^2.

Table S4 The photophysical properties and electrochemical data of BCP-BP-DMAC and calculated energy levels.

Compound	λ_{abs} [a] [nm]	λ_{PL} [a] [nm]	$E_{Ox}^{1/2}$ [b] [V]	HOMO [c] [eV]	LUMO [c] [eV]	Eg [d] [eV]
BCP-BP-DMAC	250,300	535	0.98	-5.4	-2.41	2.99

[a] Tested for molecules in DCM solutions. [b] Potential was versus Ag/Ag^{+}. [c] Ferrocene couple (Fc/Fc^{+}) was used as the internal reference. [c] The energy levels were calculated using the following equations: $E_{HOMO} = -(E_{Ox1/2} - E_{Fc/Fc+} + 4.8)$ eV, $E_{LUMO} = E_g + E_{HOMO,}$ [d] The optial energy calculated using the equations: $E_g = 1240/\lambda_{abs(onset)}$

Table S5 Summary of some critical parameters of these different NPs.

NPs: i.e. BCP-BP-DMAC:PSMA (w/w)	**λ_{PL} [a] (nm)**	**τ_{PF}/τ_{DF} [a] (ns/μs)**	**Φ_{PL}[a] (%)**	**Ret[a] (Ω)**	**Θw[a] (°)**	**Φ_{ECL}[b] (%)**
Bare AIDF NPs	503	15.39/0.79	18.45	656	78.66	1.00
2:1	505	15.36/0.79	23.26	3903	62.37	1.66
1:3	503	15.94/1.04	29.31	4685	58.54	127
1:5	502	15.08/1.35	30.80	8484	55.49	75.7

[a] Test under ambient atmosphere conditions. [b] The relative ECL efficiency (i.e. Φ_{ECL}) calculated for these NPs in PBS media containing 50 mM TEOA as a a coreactant (Φ_{ECL} of bare BC-BP-DMAC NPs was taken as 1.00 as a reference).

Reference

1. H. Chen, H. Liu, Y. Xiong, J. He, Z. Zhao and B. Z. Tang, *Mater. Chem. Front.*, 2022, **6**, 924-932.
2. X. Zou, Z. Zeng, B. Zhao, Y. Yue, Z. Xu, Y. Zhang, Y. Fu, Z. Xie, L. Niu and B. Zhang, *ACS Appl. Polym. Mater.*, 2023, **5**, 10116-10126.
3. Y. Luo, B. Zhao, B. Zhang, Y. Lan, L. Chen, Y. Zhang, Y. Bao and L. Niu, *Analyst*, 2022, **147**, 2442-2451.
4. Z. Wang, Y. Feng, N. Wang, Y. Cheng, Y. Quan and H. Ju, *J. Phys. Chem. Lett.*, 2018, **9**, 5296-5302.
5. T. Lu and F. W. Chen, *J. Comput. Chem.*, 2012, **33**, 580-592.
6. H. L. Fei, J. C. Dong, M. J. Arellano-Jiménez, G. L. Ye, N. D. Kim, E. L. G. Samuel, Z. W. Peng, Z. Zhu, F. Qin, J. M. Bao, M. J. Yacaman, P. M. Ajayan, D. L. Chen and J. M. Tour, *Nat. Commun.*, 2015, **6**, 8668.
7. B. L. Zhao, Y. L. Luo, X. D. Qu, Q. Hu, J. H. Zou, Y. He, Z. B. Liu, Y. W. Zhang, Y. Bao, W. Wang and L. Niu, *J. Phys. Chem. Lett.*, 2021, **12**, 11191-11198.
8. S. Wang, H. Zhang, B. Zhang, Z. Xie and W.-Y. Wong, *Mater. Sci. Eng. R.-Rep.*, 2020, **140**, 100547.
9. B. Zhang, Y. Kong, H. Liu, B. Chen, B. Zhao, Y. Luo, L. Chen, Y. Zhang, D. Han, Z. Zhao, B. Z. Tang and L. Niu, *Chem. Sci.*, 2021, **12**, 13283-13291.